



The effect of a double $n(\text{O}) \rightarrow \pi^*(\text{C}=\text{O})$ intramolecular interaction on the stability of 3-nitrophthalic acid

When the weaks beat an intramolecular hydrogen bond

Lorena Monterrosas-Pérez¹ · Jacinto Sandoval-Lira^{2,3} · M. P. Amador-Ramírez¹ · H. Flores-Segura¹ · Julio M. Hernández-Pérez¹ · J. M. Solano-Altamirano¹

Received: 26 May 2019 / Accepted: 10 July 2019 / Published online: 5 August 2019
© Springer Science+Business Media, LLC, part of Springer Nature 2019

Abstract

It is not frequent that weak non-covalent interactions counteract moderate hydrogen bonds. And it is also very uncommon to observe two concurrent $n \rightarrow \pi^*$ interactions, much less involving the same acceptor atom. In this work, we performed a theoretical analysis over all stable conformers of the 3-nitrophthalic acid. This compound has such a rich conformational variety, that it allowed us to compare different stabilizing and destabilizing effects as a function of a few dihedral angles. We found that the lowest-energy structure is the result of a balance between the stabilization provided by a double $n \rightarrow \pi^*$ interaction, the global decrease of steric repulsions, and alteration of the electron delocalization. The contributions of these entities to the global molecular stability are coupled (i.e., all are affected when one is modified) in such a manner that the formation of a double $n \rightarrow \pi^*$ interaction is preferred over the formation of a moderate hydrogen bond.

Keywords Weak non-covalent interaction · 3-Nitrophthalic acid conformers · Hydrogen bonding

Introduction

Understanding the structure of molecules is one of the main tasks of a chemist. Naturally, this understanding improves our ability to predict and ultimately control chemical reaction outcomes, as well as to understand chemical properties. This, in turn, enhances our understanding of much more complex phenomena observed in synthetic organic chemistry, structural biology, etc. In addition to the well-known concept of chemical bonding, which has been around for more than a century, more complex models have been developed. In this context, recently $n \rightarrow \pi^*$ interactions have

attracted the attention of the scientific community, because of both their role in stabilizing biomolecular and material structures, and their influence on biological processes [1, 2, and references therein]. These $n \rightarrow \pi^*$ interactions, whose origins can be traced back to the work of Bürgi-Dunitz [3], are commonly present in nucleophilic additions to carbonyl groups, and are considered weak because the energies typically associated with these intermolecular (intramolecular) interactions are $\sim 1 \text{ kcal mol}^{-1}$ ($< 3 \text{ kcal mol}^{-1}$). Weak as might they be, these interactions may alter the reactivity of compounds [4] and are crucial for the conformational stability of proteins [5, 6].

However, $n \rightarrow \pi^*$ interactions are important not only in biological systems, wherein the weak intermolecular interactions drive the outcomes and properties, but also in isolated molecules. For instance, they have been found to be present in siloxanes, germoxanes, and stannoxanes [7], wherein they determine the geometry of the E-O-E moiety (E=Si, Ge, Sn). Furthermore, $n \rightarrow \pi^*$ interactions are also ubiquitous in the stability of single molecules and even in diastereoselective synthetic designs [8]. In Ref. [8], our research group has shown that an $n_{\text{O}} \rightarrow \pi^*_{\text{C}=\text{O}}$ interaction provides enough thermodynamic stability to lock the conformation of a reaction intermediate compound,

Electronic supplementary material The online version of this article (<https://doi.org/10.1007/s11224-019-01399-6>) contains supplementary material, which is available to authorized users.

✉ Julio M. Hernández-Pérez
julio.hernandez@correo.buap.mx

✉ J. M. Solano-Altamirano
jmsolanoalt@gmail.com

Extended author information available on the last page of the article.

which ultimately renders a stereocontrolled construction of the naturally occurring cephalosporolide E.

On the other hand, hydrogen bonding is another widely studied non-covalent weak interaction, which is present in a plethora of chemical and biological systems (see 9, 10, and references therein for a general overview of hydrogen bonding). To our purposes, we highlight the hydrogen bond contribution to determining structural properties of molecules [11], and to driving organic reaction outcomes [12, 13]. In this context, our research group has found that intramolecular hydrogen bonding, occurring within intermediates of organic reactions, should be included in synthetic plan designs.

The phenomenon that inspired this work was found while we were computing thermochemical properties of the nitrophthalic acid isomers [11]. In Ref. [11], the theoretical and experimental enthalpies of formation in gas-phase were determined. Theoretically, the enthalpies were calculated using a Boltzmann weighted average, for which a conformational search of each isomer was considered. Our theoretical estimations were in great agreement with the experimental determinations (they differ by less than 1 kcal mol^{-1}), and the difference was found to be within experimental uncertainties. Certainly, during this search we encountered a very rich conformational diversity for each isomer, and in particular we found that one of the conformers of the 3-nitrophthalic acid (3NFAc, Fig. 1) presented an intramolecular hydrogen bond. Naturally, we expected this conformer to be the lowest-energy structure of the set; however, and quite surprisingly, we realized that the conformer with hydrogen bonding was not the structure with the least electron energy at 0 K. In fact, the (G4) energy difference between the global lowest-energy conformer and the lowest-energy conformer that had an intramolecular hydrogen bond was nearly 3 kcal mol^{-1} . This energy difference suggested us that there should exist some competition between hydrogen bonds and other interactions, such as $n \rightarrow \pi^*$, electron repulsion, and electron delocalization, which determine the conformer stable structures of the 3NFAc. The most intriguing aspect is “to what extent?” In this work, we perform a theoretical study of different interactions and chemical phenomena present in the 3NFAc. We will show that the structure of the most stable conformer cannot be explained through a few dominant interactions, but through a cooperative

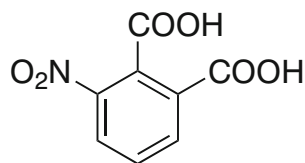


Fig. 1 The 3-nitrophthalic acid (3NFAc)

compromise between the increasing of weak stabilizing contributions and the decrease of un-stabilizing effects, all of this occurring in a non-local fashion.

We must remark here that the competition between, and mutual influence of, $n \rightarrow \pi^*$ interactions and hydrogen bonds has been discussed in previous works [14, 15], although the systems were comprised of molecular complexes, as opposed to single molecules. Also, some discussion have been published regarding the aversion of a system to form double $n \rightarrow \pi^*$ interactions [16], i.e. according to Choudhary et al., once an $n \rightarrow \pi^*$ interaction has been formed, a second should be disfavored. In this context, the 3NFAc constitutes a very interesting case, wherein some effects behave oppositely to what has been observed in molecular complexes.

A pragmatic summary of NBO, QTAIM, and NCI

Given the properties of the interactions present in the 3NFAc, we will use different methodologies to analyze weak interactions, namely, the Natural Bond Orbital (NBO) theory [17–19], the Quantum Theory of Atoms in Molecules (QTAIM) [20], and the Non-Covalent Interaction (NCI) index [21]. This will allow us to enhance our perspective of the different competing interactions, from different viewpoints.

In what follows, we will state, quite briefly and exclusively in relation to our purposes, the main practical aspects of the NBO, QTAIM, and NCI methodologies, and their relation to weak non-covalent interactions and hydrogen bonds. The interested reader is referred to [22–24] for further details.

The most popular method, to the best of our knowledge, for studying $n \rightarrow \pi^*$ interactions is the NBO analysis. In NBO theory, the wavefunction is expanded by molecular orbitals that maximize the resemblance to the Lewis electron pairs (filled orbitals) and the Rydberg orbitals (unoccupied orbitals). In this manner, we can describe, in familiar terms, the interactions of a molecule [22]. For instance, the electron delocalization between a lone electron pair (of a donor atom) and an unoccupied antibonding orbital (or an acceptor), i.e., an $n \rightarrow \pi^*$ interaction, or the hydrogen bond, which occurs between a lone electron pair (of the donor atom), and the σ^* antibonding orbital of the hydrogen atom (this interaction is denoted as $n \rightarrow \sigma^*$). Furthermore, within the NBO framework, it is possible to estimate the delocalization energy associated with the overlap between the orbitals of the donor and the acceptor atoms. Such delocalization energy is obtained from a second order perturbation approach given by

$$\Delta E_{ij}^{(2)} = q_i \frac{F^2(i, j)}{\varepsilon_i - \varepsilon_j}. \quad (1)$$

In Eq. 1, q_i is the occupancy number of the orbital i , $F(i, j)$ are the Fock matrix elements, and $\varepsilon_i \equiv F(i, i)$. Qualitatively, the overlap between NBO orbitals indicates the existence of the interaction, and quantitatively, the strength of an interaction increases as the delocalization energy, $\Delta E_{ij}^{(2)}$, increases. With the NBO methodology, one can also estimate the steric contributions to the energy of a molecule. In practical terms, this is done by comparing, against a reference system, the sum of steric exchange energy contributions, $E^{(sx)} = \sum \Delta E_{ij}^{(sx)}$. Here, $\Delta E_{ij}^{(sx)}$ stands for the energy associated with steric repulsion between the i and j natural localized molecular orbitals. These $\Delta E_{ij}^{(sx)}$ contributions are estimated by computing the kinetic energy pressures between i and j orbitals [22]. Notice that the net repulsion/attraction effect between two atoms in a molecule is the sum of several $\Delta E_{ij}^{(sx)}$'s and several $\Delta E_{ij}^{(2)}$'s.

The QTAIM constitutes another popular and robust method to analyze the properties of a molecule. QTAIM is heavily based on the topological properties of the electron density, ρ [20, 23, 25]. In practical terms, one characterizes, through several fields functionals of ρ , the critical points (CPs) of the electron density (i.e., those points where $\nabla\rho = \mathbf{0}$). Since ρ is a function defined on the physical 3D space, there are four types of CPs, which can be uniquely characterized by the signs of the Hessian eigenvalues at the CPs. To our purposes, the most salient CPs are those which are (a) maxima in three directions and (b) maxima in two directions and minima in one direction. In the literature, these CPs are referred to as (a) attractor CPs (ACPs) and (b) bond CPs (BCPs) or line CPs (in this work we will use the first name, i.e., BCPs). In addition, there exists special gradient paths that connect ACPs and BCPs, which are commonly called bond gradient paths (BGPs). Apart from some pathological cases, the existence of a BGP indicates the presence of an interaction between two atoms, although the discussion about whether or not BGPs can be considered chemical bonds is still open. Nevertheless, QTAIM is a very useful theoretical framework to confirm the formation of hydrogen bonds, which are known to be characterized by both the existence of a BGP between a donor and hydrogen atoms, and by the values of ρ and $\nabla^2\rho$ at the BCP. Certainly, Koch and Popelier conducted an extensive characterization of systems having hydrogen bonds, from which they observed that a hydrogen bond is present if $\rho_{BPC} \in [0.002, 0.040]$ and $\nabla^2 \in [0.024, 0.139]$, approximately [26]. In addition, the values of ρ_{BPC} can provide an estimate of the bond strengths, which in practical terms can be stated as the greater ρ_{BPC} the greater the bond strength, in particular if one compares two similar interactions [27, 28]. The properties of the electron density along the BGP can also be used to qualitatively describe the electron delocalization between two neighboring atoms.

To this end, one can analyze the Hessian eigenvalues along the BGP, and specifically the ratio between the two negative eigenvalues of the Hessian,

$$\varepsilon(\mathbf{r}) \equiv \frac{\lambda_1(\mathbf{r})}{\lambda_2(\mathbf{r})} - 1. \quad (2)$$

Here, λ_1 and λ_2 are the first and second eigenvalues (in ascending order), and ε is called ellipticity. The greater ε is, the greater the electron delocalization, and roughly speaking the ellipticity measures the π character of a bond. In addition, the complete profile of the ellipticity upon the bond path also provides insight on the bond properties [29, 30].

Sometimes, however, the interactions (in particular hydrogen bonds) in a molecule are so weak that there is no BGP between the interacting atoms [31, 32]. In such cases, very weak interactions (including non-covalent interactions) can be better characterized using the Non-Covalent Interaction (NCI) index. This index is also based on the mathematical properties of the electron density, and relies on the so-called reduced density gradient, s , which is defined as

$$s \equiv \frac{1}{2} \frac{|\nabla\rho|}{(3\pi^2)^{1/3} \rho^{4/3}}, \quad (3)$$

and a field defined as

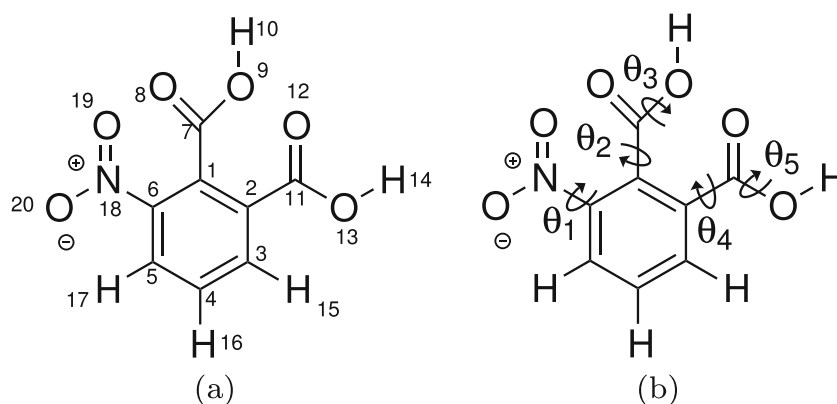
$$\Lambda \equiv \text{sign}(\lambda_2)\rho. \quad (4)$$

In Eq. 4, λ_2 is the second Hessian eigenvalue (in ascending order). This index offers, qualitatively, a visual representation of weak interactions that may be as weak as van der Waals' (obviously hydrogen bonds are also included in this set), which is obtained by mapping the field Λ onto isosurfaces of s . This map provides also a method to identify whether the interaction is repulsive or attractive [24, 33]; thus, steric repulsions between two atoms within a molecule can also be qualitatively identified. The latter can be done by looking at the sign of Λ : in pragmatic terms, if $\Lambda < 0$ then the interaction is considered attractive, and repulsive otherwise.

Computational details

Our convention for numbering the atoms of the 3NFAC is shown in Fig. 2a. Initial geometries were generated by constructing a basic geometry following the scheme shown in Fig. 2b. The dihedral angles $\theta_1 - \theta_5$ were set so as to render the conformer labeled as A1 in Fig. S1 of the Supporting Information. The rest of the initial geometries shown in Fig. S1 of the Supporting Information were generated by rotating the dihedral angles $\theta_1 - \theta_5$, which were

Fig. 2 **a** Atom numbering convention and **b** definition of dihedral angles of the 3-nitrophthalic acid, as used in this work



set to be $\sim 0^\circ$ or $\sim 180^\circ$, accordingly. Subsequently, these initial geometries were optimized, as described below. The electron densities (extracted from wavefunction files) were requested after optimizations and saved for later analyses.

Unless specified otherwise, calculations were carried out using the second-order perturbation theory (MP2) and the cc-pVTZ basis set. Geometry optimizations were conducted using GAMESS program (version 2013-R1) [34]. Minimum energy geometries were confirmed via frequency analyses, and all minima showed real frequency eigenvalues. To study electronic interactions and bonding, natural bond orbital (NBO) theory analyses were performed, using the program NBO6 [35], coupled with GAMESS (version 2013-R1). The NBO analyses were always computed on optimized geometries, using the MP2 non-relaxed density, and 0.05 a.u. isosurfaces for every plot wherein we depict NBO orbitals. Chemcraft 1.617 was used to visualize them [36]. Steric effects were requested through the STERIC keyword of NBO program. The analysis of the electron density, based on the Quantum Theory of Atoms in Molecules (QTAIM) and the index of Non-Covalent Interactions (NCI), was obtained from the Denstoolkit suite [37], which relies on PovRay [38] (QTAIM) and VMD [39] (NCI) for visualization purposes.

Results and discussion

Geometries and total energies

In Fig. 3, we show the 3D view of the optimized structures of the 3NFAC's conformers, as well as the definition of the labels we will use hereon. The labels $\{\mathbf{A1}, \dots, \mathbf{H2}\}$ are not representative of the electron energy order, and conformers that have intramolecular hydrogen bonds are marked with a star. Also, in Fig. 3, we show some relative energies, given in kcal mol^{-1} , that are required to pass from left to right column or from upper to lower row. E.g., passing from $\mathbf{A2}$ to $\mathbf{A1}$ requires $-0.04 \text{ kcal mol}^{-1}$ (i.e., $\mathbf{A1}$ has a lower energy),

or passing from $\mathbf{C2}$ to $\mathbf{D2}$ requires $1.14 \text{ kcal mol}^{-1}$ (i.e., $\mathbf{C2}$ has a lower energy).

In Table 1, we list the total electron energies (which include zero point corrections), ΔE_I , $I \in \{\mathbf{A1}, \dots, \mathbf{H2}\}$, relative to the lowest-energy conformer $\mathbf{A1}$. The order of the items reflects the same order provided in Fig. 3 for easing the relation between energies and structures. For future reference, $\mathbf{E1}$ is the conformer that has a hydrogen bond and that is closest in energy to $\mathbf{A1}$.

In Table 2, we list the dihedral angles, relevant to this work, that define the 3NFAC's conformers, i.e., $\theta_1 - \theta_5$, see also Fig. 2b. The complete set of geometries is given in the Supporting Information, Tables S2–S17.

The conformer $\mathbf{A1}$ (whose initial geometry was inspired by our previous findings [11]) has the lowest electron energy of the complete set; however, we found that the optimized structure at the B3LYP/6-31G(2df,p) theory level, which was used in [11], is different from the structure obtained at the MP2/cc-pVTZ theory level. The RMDS between these structures is 0.26 \AA , and the discrepancy stems from how the methods account for dispersion effects, which originates different deviations from planarity of the $-\text{NO}_2$ group, relative to the benzenic ring. The dihedral angle θ_1 obtained from MP2/cc-pVTZ is -147.1° (i.e., the $-\text{NO}_2$ is deviated 32.9° from the benzene plane), and from B3LYP/6-31G(2df,p) is -172.6° (i.e., the $-\text{NO}_2$ is deviated 7.4° from the benzene plane). These results are consistent with what has been found for the nitroxoline [40]. In the latter work, Tikhonov et al. argued that this tilt is caused by the competition between a π - π interaction and the repulsion of the $-\text{NO}_2$ group and an adjacent hydrogen (see Fig. 4).

In the 3NFAC case, and looking at Table 2, we observe that the $-\text{NO}_2$ group deviates from planarity between 24.8° ($\mathbf{E2}$) and 51.1° ($\mathbf{H2}$). In contrast to the nitroxoline case, we will show that the tilt observed in the 3NFAC is due not to the competition of $-\text{NO}_2/\text{H}$ repulsion and π - π interaction, but rather a balance between the π - π interaction, the repulsion stemming from adjacent oxygens (belonging to the $-\text{NO}_2$ and $-\text{COOH}$ groups), and an attractive $n \rightarrow \pi^*$ interaction

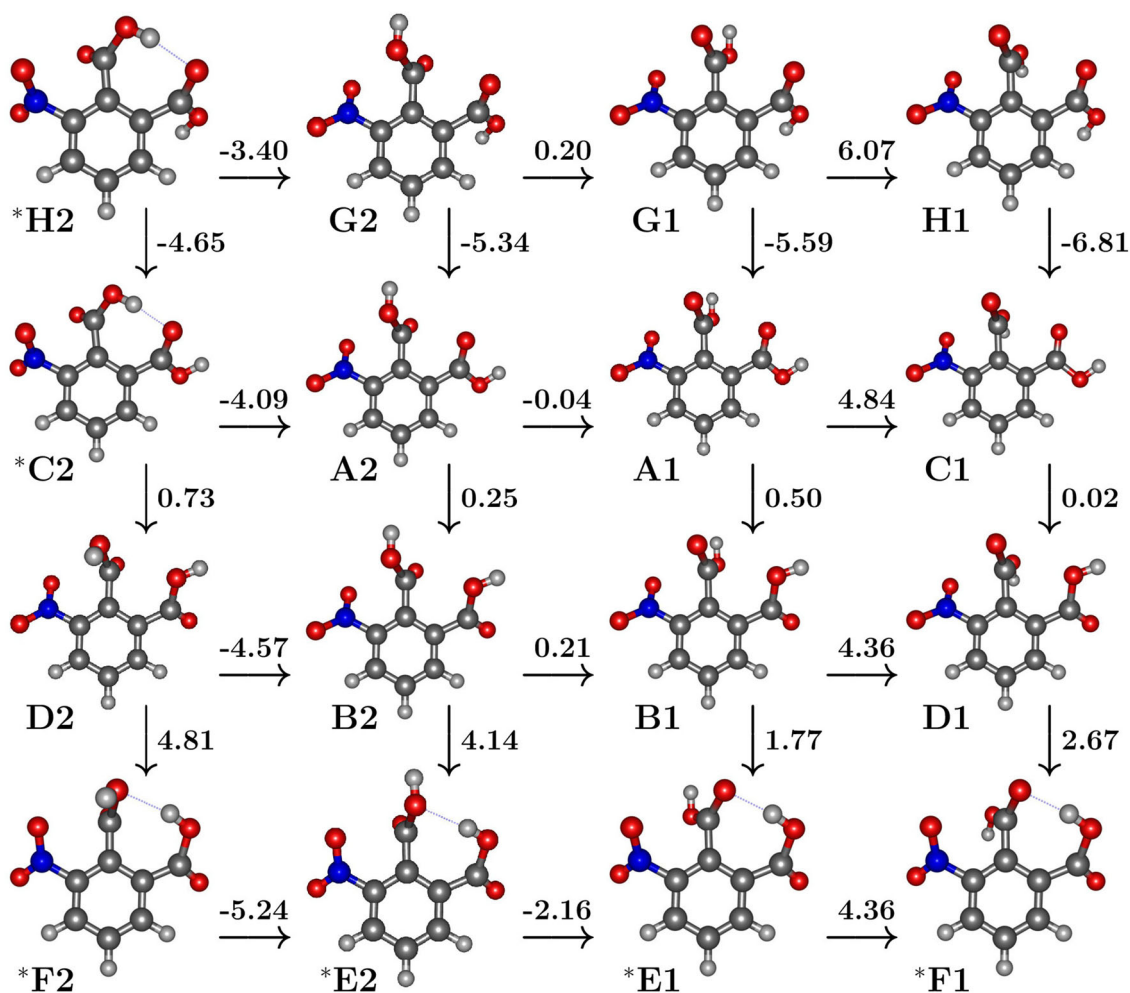


Fig. 3 Optimized structures of the 3-nitrophthalic acid's conformers and some relative energies between them. The relative energies (given in kcal mol⁻¹) above of or right to the arrows should be interpreted

between O19 and C7. This balance of forces renders a greater planarity deviation compared with the nitroxoline's and other molecules' deviations, wherein the $n \rightarrow \pi^*$ interaction is not present.

Table 1 Total electron energy differences, ΔE_I , relative to the most stable conformer **A1**, i.e. $\Delta E_I \equiv E_I - E_{A1}$ (kcal · mol⁻¹)

Structure	*H2	G2	G1	H1
ΔE_I	8.78	5.38	5.59	11.65
Structure	*C2	A2	A1	C1
ΔE_I	4.13	0.04	0.00	4.84
Structure	D2	B2	B1	D1
ΔE_I	5.28	0.29	0.50	4.86
Structure	*F2	*E2	*E1	*F1
ΔE_I	9.67	4.43	2.27	7.49

The table reflects the same order shown in Fig. 3. The stars mark the conformers that have intramolecular hydrogen bonds (see also Fig. 3)

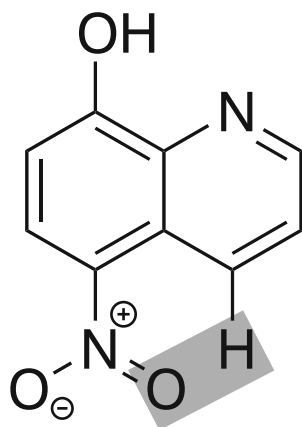
as the energy cost of passing from the left to right conformer, of from the upper to lower conformer. Conformers with hydrogen bonds are marked with a star

In Table 3, we list several geometric parameters (distances and angles) that are relevant for the following sections. However, we can already see that, considering only geometric arguments, the conformers ***C2**, ***E1**, ***E2**, ***F1**, ***F2**, and ***H2** have intramolecular hydrogen bonds (of type O–H···O). Here, we follow the recommendations provided by Jeffrey [10] and Steiner [41], who suggest that if the distance between the donor and the hydrogen atoms is (1.5–2.2) Å and the angles X–H···A > 130°, then the bond can be considered a moderate hydrogen bond (here A and X are the acceptor and the donor atoms, respectively). Certainly, the respective bond distances in the above conformers are between 1.73 Å and 1.90 Å, and the angles X–H···A are between 146.5 and 161.9° (see Table 3); therefore, these hydrogen bonds are moderate. According to Steiner's classification [41], the hydrogen bond energies of the conformers should be between 4 and 15 kcal mol⁻¹. At first sight, if we only consider isolated interactions, then conformers with hydrogen bonding should have had

Table 2 Dihedral angles associated with the relevant interactions present in the 3-nitrophthalic acids' conformers (see also Fig. 2)

Structure	*H2	G2	G1	H1	*C2	A2	A1	C1
θ_1 (C5C6N18O19)	128.9	− 145.1	− 143.1	− 143.1	129.5	− 148.4	− 147.1	− 146.0
θ_2 (C2C1C7O8)	127.0	60.2	− 115.0	− 106.6	126.5	67.4	− 106.5	− 95.9
θ_3 (O8C7O9H10)	− 166.2	2.0	3.2	− 171.9	− 163.9	1.4	2.5	− 175.4
θ_4 (C3C2C11O12)	− 131.3	− 130.8	− 135.0	138.4	− 142.1	− 150.9	− 159.5	− 178.0
θ_5 (O12C11O13H14)	− 173.2	171.1	− 171.5	− 172.4	0.5	0.3	0.8	0.6
Structure	D2	B2	B1	D1	*F2	*E2	*E1	*F1
θ_1 (C5C6N18O19)	− 153.7	− 144.8	− 144.6	− 143.5	153.1	155.2	141.0	147.5
θ_2 (C2C1C7O8)	68.4	62.5	− 110.2	− 103.8	89.6	98.1	− 56.7	− 62.4
θ_3 (O8C7O9H10)	− 173.8	3.9	− 0.2	− 171.5	158.4	2.9	− 4.9	175.0
θ_4 (C3C2C11O12)	31.5	32.1	26.7	22.9	23.5	29.6	27.4	29.6
θ_5 (O12C11O13H14)	5.8	4.8	2.7	2.6	− 176.1	− 175.7	177.3	177.4

the lowest total electron energy (it is not very usual that weak non-covalent interactions contribute with more than a very few kcal mol^{−1}). However, the most stable conformer **A1** does not have hydrogen bonding, and its energy is 2.27 kcal mol^{−1} lower than ***E1**. Hence, different interactions must occur, and furthermore, the interactions must overcome the stabilizing effect of an intramolecular hydrogen bond. Thus, in the following sections, we analyze diverse non-covalent interactions that occur between the atoms O19, O12, O13, O8, H10, H14, H15, H17, and C7, for the different conformers of the 3NFAC. Also, for completeness purposes, we repeated the calculations presented here, but using the x-ray geometry [42] and partial optimizations of it. In Table S1 of the Supplementary Information, we list the geometric properties (and additional properties) of these structures, which we will discuss later.

**Fig. 4** The nitroxoline and the repulsive interaction (gray rectangle) that precludes the $-\text{NO}_2$ coplanarity with the ring

NBO analysis

The NBO analysis confirmed the presence of $n \rightarrow \pi^*$ interactions, as well as hydrogen bond interactions (of the type $n \rightarrow \sigma^*$). From Table 3, we see that the distances $\text{O19} \cdots \text{C7}$ or $\text{O12} \cdots \text{C7}$ are between 2.63 Å and 2.81 Å, whereas the angles $\text{O19}-\text{C7}=\text{O8}$ and $\text{O12}-\text{C7}=\text{O8}$ are between 80.4 and 108.8°. According to Bürgi-Dunitz [3], the previous distances and angles suggest that the C7 atom is prone to nucleophilic attacks. The question here is which is the group acting as a nucleophile through an $n \rightarrow \pi^*$ interaction, the $-\text{NO}_2$ or the $-\text{COOH}$? The answer is both; in some conformers, they both act as nucleophiles concurrently. This is, in part, opposed to the findings reported by Choudhary et al. [16], wherein the authors conclude that once an intermolecular $n \rightarrow \pi^*$ interaction is formed, then a second interaction of the same type should be disfavored. The presence of double intramolecular $n \rightarrow \pi^*$ interactions is one of the most intriguing features of the 3NFAC. We will further elaborate on this throughout our discussion.

The fact that both nitro and carboxyl groups act as nucleophiles (sometimes concurrently) can already be seen from the pyramidalization suffered by the central C1–COOH moiety, which is another geometric feature that indicates the presence of an $n \rightarrow \pi^*$ interaction. Considering that in some conformers there are two concurrent $n \rightarrow \pi^*$ interactions, we measured the pyramidalization through a parameter p , whose magnitude is the perpendicular distance of C7 from the plane formed by C1–O8–O9 (the greater the distance, the greater the pyramidalization). Also, if p , shown in Table 3, is positive (negative), then the carbon C7 lifts from the plane towards the $-\text{COOH}$ ($-\text{NO}_2$) group. From Table 3, we can see that in **A1** pyramidalization is very low ($p = + 0.003$ Å, towards the $-\text{COOH}$ group);

Table 3 Geometric parameters of the relevant non-covalent interactions present in the conformers of 3-nitrophthalic acid

Parameter	*H2	G2	G1	H1	*C2	A2	A1	C1
C7=O8 (Å)	1.21	1.20	1.20	1.20	1.21	1.20	1.21	1.20
O19...C7 (Å)	2.81	2.68	2.68	2.66	2.81	2.64	2.63	2.65
O19-C7=O8 (°)	80.4	107.7	89.4	95.3	80.5	102.8	93.2	100.7
O12...C7 (Å)	–	2.86	2.83	2.77	–	2.72	2.69	2.67
O12-C7=O8 (°)	–	87.7	104.9	101.6	–	89.1	102.4	102.4
H10...O12 (Å)	1.78	–	–	–	1.75	–	–	–
O9-H10...O12 (°)	146.5	–	–	–	147.3	–	–	–
p (Å)	+ 0.005	– 0.011	– 0.005	– 0.001	+ 0.007	– 0.003	+ 0.003	+ 0.007
Parameter	D2	B2	B1	D1	*F2	*E2	*E1	*F1
C7=O8 (Å)	1.20	1.20	1.21	1.20	1.20	1.20	1.22	1.21
O19...C7 (Å)	2.61	2.65	2.63	2.64	2.56	2.54	2.65	2.61
O19-C7=O8 (°)	102.9	105.1	91.6	96.9	105.0	95.9	108.8	105.9
O13...C7 (Å)	2.68	2.71	2.68	2.66	–	–	–	–
O13-C7=O8 (°)	94.6	89.4	101.3	98.8	–	–	–	–
H14...O9 (Å)	–	–	–	–	1.90	1.86	–	–
O13-H14...O9 (°)	–	–	–	–	161.9	152.8	–	–
H14...O8 (Å)	–	–	–	–	–	–	1.73	1.75
O13-H14...O8 (°)	–	–	–	–	–	–	153.7	153.4
p (Å)	– 0.013	– 0.008	– 0.002	– 0.006	– 0.054	+ 0.022	– 0.016	– 0.022

Distances are given in Å, and dihedral angles in degrees. The magnitude of the parameter “p” is the perpendicular distance between C7 and the plane formed by O8–O9–C1, and a positive (negative) sign of p indicates that C7 lifts from the plane towards the –COOH (NO₂) group. Conformers that have hydrogen bonds are marked with stars

hence, the –COOH group is barely a stronger nucleophile than the –NO₂ group in this conformer. On the other hand, the pyramidalization of ***E1** is greater, relative to **A1** (p = – 0.016 Å), and C7 lifts towards the –NO₂ group because the –COOH group is engaged in forming a hydrogen bond.

In Fig. 5, we depict the overlap of the NBO orbitals associated with the $n_{O19} \rightarrow \pi_{C7=O8}^*$ and $n_{O12} \rightarrow \pi_{C7=O8}^*$ interactions. Both are concurrently present in **A1**, and they appear as well in the rest of the conformers in different combinations, i.e., the double $n \rightarrow \pi^*$ interaction is by no means unique to **A1**. Figure 5 offers the first qualitative confirmation that both $n \rightarrow \pi^*$ interactions exist simultaneously.

The $n \rightarrow \pi^*$ and $n \rightarrow \sigma^*$ interactions strength

Table 4 lists the second-order perturbation energies, $\Delta E_{ij}^{(2)}$ (hereon denoted simply as $E^{(2)}$, see Computational Details), for some non-covalent interactions existing in each one of the 3NFAc's stable conformers. **G2**, **G1**, **H1**, **A2**, **A1**, **C1**, **D2**, **B2**, **B1**, and **D1** have two $n \rightarrow \pi^*$ interactions, and each individual interaction includes the carbonyl group (C7=O8). In such conformers, the respective $E^{(2)}$ of the $n_{O19} \rightarrow \pi_{C7=O8}^*$ interaction (denoted in Tables and Figures as NBO₁) is 1.61–2.71 kcal mol^{–1}. In conformers **G2**, **G1**,

H1, **A2**, **A1**, and **C1**, the $E^{(2)}$ of the $n_{O12} \rightarrow \pi_{C7=O8}^*$ interaction (denoted in Tables and Figures as NBO₂) is between 0.72 and 2.77 kcal mol^{–1}. On the other hand, in each one of conformers **D2**, **B2**, **B1**, and **D1**, there exists an $n_{O13} \rightarrow \pi_{C7=O8}^*$ (denoted in Tables and Figures as NBO₄), whose $E^{(2)}$ is 1.53–2.36 kcal mol^{–1}. According to the above discussion, the –NO₂ group in conformers **G2**, **G1**, **H1**, **A2**, **D2**, **B2** and **B1** is a stronger nucleophile, relative to conformers **A1**, **C1** and **D1**. The –COOH group has the opposite trend.

As to the ***H2**, ***C2**, ***F2**, ***E2**, ***E1**, and ***F1** conformers, each of these shows two interactions that can be associated with weak non-covalent interactions of the kinds NBO₁ and $n \rightarrow \sigma^*$ (the $n_{O8} \rightarrow \sigma_{O13-H14}^*$ is denoted as NBO₅ and $n_{O9} \rightarrow \sigma_{O13-H14}^*$ as NBO₆). The $E^{(2)}$'s of the NBO₁ interactions are between 0.28 and 4.22 kcal mol^{–1}, and the $E^{(2)}$'s of NBO₅ and NBO₆, which are associated with O–H...O contacts, are between 6.53 and 10.20 kcal mol^{–1} (see Table 4). This confirms that these hydrogen bonds are moderate. Figure 5 c and d show the NBO orbital overlaps of the NBO₁ and NBO₅ interactions present in ***E1**, whereas the interactions present in the rest of the conformers are depicted in Fig. S2 of the Supporting Information.

In the 3NFAc's conformer **A1**, the $E^{(2)}$ energies of the two $n \rightarrow \pi^*$ interactions are 2.30 kcal mol^{–1} (NBO₁)

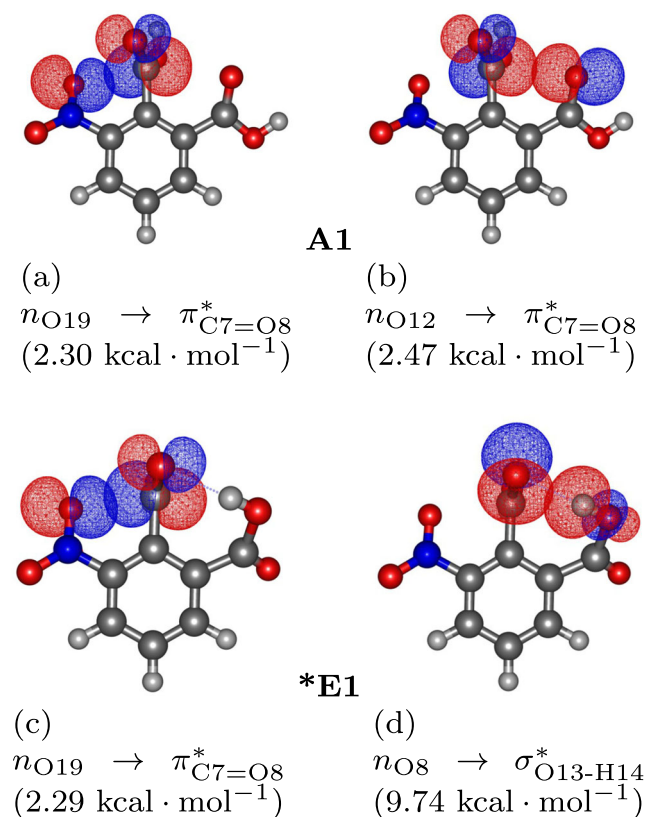


Fig. 5 Relevant NBO interactions in conformers **A1** (upper row) and ***E1** (lower row)

and 2.47 kcal mol⁻¹ (NBO₂), respectively, rendering a total contribution of 4.77 kcal mol⁻¹ (see Table 4). (The difference $E^{(2)}(n_{O19} \rightarrow \pi_{C7}^*) - E^{(2)}(n_{O12} \rightarrow \pi_{C7}^*) = 0.17$ kcal · mol⁻¹; therefore, both interactions have similar strength. This is consistent with the conclusions drawn from the pyramidalization parameter p , see Table 3, i.e., the NBO₁ interaction is barely weaker than the NBO₂ interaction. On the other hand, in **E1** the interactions NBO₁ (with $E^{(2)} = 2.29$ kcal mol⁻¹) and NBO₅ (with $E^{(2)} = 9.74$ kcal mol⁻¹) render a total contribution of

Table 4 Second-order perturbation energies, $E^{(2)}$ (kcal mol⁻¹), of the relevant NBO interactions present in the conformers of 3-nitrophthalic acids. Conformers that have hydrogen bonds are marked with stars

Interaction	*H2	G2	G1	H1	*C2	A2	A1	C1
NBO ₁ $n_{O19} \rightarrow \pi_{C7=O8}^*$	0.56	2.17	1.64	1.62	0.28	2.71	2.30	1.92
NBO ₂ $n_{O12} \rightarrow \pi_{C7=O8}^*$	–	0.72	1.05	1.44	–	1.59	2.47	2.77
NBO ₃ $n_{O12} \rightarrow \sigma_{O9-H10}^*$	10.20	–	–	–	12.53	–	–	–
Interaction	D2	B2	B1	D1	*F2	*E2	*E1	*F1
NBO ₁ $n_{O19} \rightarrow \pi_{C7=O8}^*$	3.19	2.54	2.31	2.00	3.70	4.22	2.29	2.86
NBO ₄ $n_{O13} \rightarrow \pi_{C7=O8}^*$	1.71	1.53	2.18	2.36	–	–	–	–
NBO ₅ $n_{O8} \rightarrow \sigma_{O13-H14}^*$	–	–	–	–	–	–	9.74	7.55
NBO ₆ $n_{O9} \rightarrow \sigma_{O13-H14}^*$	–	–	–	–	8.28	6.53	–	–

Table 5 Energy differences (in kcal · mol⁻¹) associated with steric effects, $\Delta E_I^{(sx)}$, relative to the conformer **A1**. Here $\Delta E_I^{(sx)} \equiv E_I^{(sx)} - E_{A1}^{(sx)}$, see also Computational Details

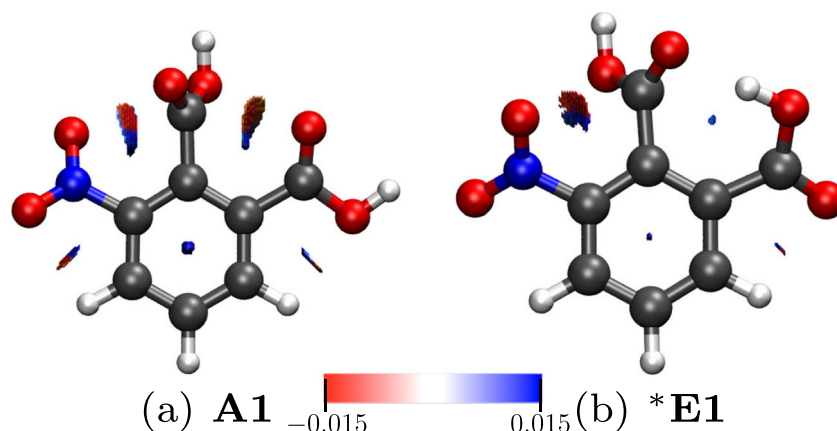
Structure	*H2	G2	G1	H1
$\Delta E_I^{(sx)}$	7.74	– 3.28	– 2.22	– 0.36
Structure	*C2	A2	A1	C1
$\Delta E_I^{(sx)}$	8.48	– 0.97	0.00	2.41
Structure	D2	B2	B1	D1
$\Delta E_I^{(sx)}$	1.40	– 3.38	– 2.19	0.83
Structure	*F2	*E2	*E1	*F1
$\Delta E_I^{(sx)}$	9.73	8.93	15.48	15.07

12.03 kcal mol⁻¹. This, in principle, is inconsistent with the observed global stabilization energy, i.e., if we compared only the sum NBO₁ + NBO₂ (**A1**) vs NBO₁ + NBO₅ (***E1**), we would have concluded that ***E1** should have had the lowest total electron energy, which is opposed to the observed total electron energies. As we discuss below, to better understand the structural features of the lowest-energy conformer **A1**, we have to consider how the presence or absence of the NBO₁, NBO₂, and NBO₅ interactions affects not only the closest neighboring bonds, but also the rest of the bonds of the 3NFAc, which in turn affects the contributions to the total electron energy. Certainly, the 3NFAc does not completely follow the rules of the group addition model.

Steric effects

In Table 5, we list the energy differences associated with the steric effects, $\Delta E_I^{(sx)} \equiv E_I^{(sx)} - E_{A1}^{(sx)}$, $I \in \{\mathbf{A1}, \dots, \mathbf{*H2}\}$, relative to **A1**. Here, $E_I^{(sx)}$ is the sum of pairwise steric contributions to the energy between natural localized molecular orbitals of conformer I (see [A pragmatic summary of NBO, QTAIM, and NCI](#) and Ref. [22] for further details).

Fig. 6 Non-Covalent Interaction index (NCI) of the conformers **a** **A1** and **b** ***E1** (color online)



The values of Table 5 should be interpreted as follows. If $\Delta E_I^{(sx)} > 0$, then the steric effects are greater in the conformer *I*. Here, we should warn the reader that the $\Delta E_I^{(sx)}$ offers an estimation of the total electronic repulsion, and tells us whether it increases or not when passing from one conformer to another. This repulsion, we must recall, should not be considered equivalent to repulsion between atoms, but between all the electrons “contained” by localized orbitals of the molecule.

As we can see, the total contribution, stemming from steric effects, is $15.48 \text{ kcal mol}^{-1}$ greater in ***E1**, compared with **A1**. This contribution overcomes the stabilization stemming from the interactions NBO_1 and NBO_5 present in ***E1**, relative to **A1**, i.e., in ***E1** the steric effects counteract the stabilization supplied by the hydrogen bond and the weak $n \rightarrow \pi^*$ interaction, in such a manner that the decreased steric effects in **A1** plus the stabilization provided by the double $n \rightarrow \pi^*$ interaction renders the conformer **A1** to have a lower total electron energy. However, the interplay between weak interactions and steric effects is not the end of this story. In what follows, we analyze additional effects present in the 3NFAC conformations.

NCI

In Fig. 6, we depict NCI plots of the conformers **A1** and ***E1**. The plates between the O19 and C7 atoms in both conformers confirms the existence of a weak non-covalent interaction. The negative sign of the Λ field in the outer region, i.e., away from the benzenic ring, indicates that such interaction is attractive. Furthermore, the NCI plate between O12 and C7, in **A1**, confirms as well the presence of a second attractive $n \rightarrow \pi^*$ interaction, and the plate between O8 and H14, in ***E1**, supports the existence of a hydrogen bond. The NCI plots for the complete set of conformers are shown in Fig. S3 of the Supporting Information.

In contrast to the observations made for the nitroxoline [40], wherein the planarity deviation of the $-\text{NO}_2$

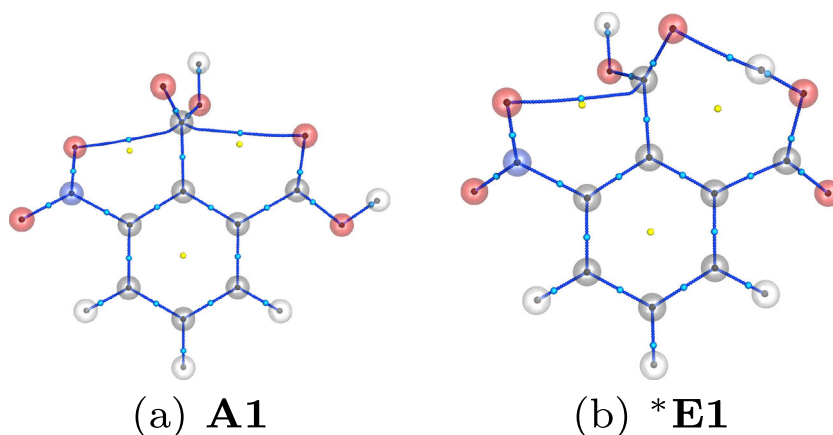
group (relative to the benzenic plane) is caused by the competition of the π - π delocalization and the repulsion between the $-\text{NO}_2$ and an adjacent hydrogen; in the 3NFAC, the deviation is caused by the competition between the attractive $n_{\text{O19}} \rightarrow \pi_{\text{C7=O8}}^*$ interaction and the electronic repulsion of O19 with O8 and O9. Both effects involve the groups $-\text{NO}_2$ and $-\text{COOH}$. On the other hand, in the 3NFAC, the interactions with adjacent hydrogens appear to be attractive (see the values of Λ at the plates between O20 and H17, as well as between O13 and H15, in Fig. 6). However, this is not conclusive because such interactions are very weak, and also because there is ring tension created by the O20-N18-C6-C5-H17 and O13-C11-C2-C3-H5 moieties, which is suggested by the positiveness of Λ close to the center of such rings.

QTAIM

In Fig. 7, we show the topology of the electron density for conformers **A1** and ***E1**. The QTAIM analysis confirms the formation of a hydrogen bond, in conformer ***E1**, between O8 and H14 atoms, which was expected. However, we bring the reader’s attention to the critical points, and gradient paths, formed between C7 and O19, of both conformers, and those formed between C7-O12, in **A1**. Since these gradient paths are associated with weak non-covalent interactions, it is not very common for QTAIM to detect them. This would suggest that the apparently weak $n \rightarrow \pi^*$ interactions are not so weak, in relation to their neighboring chemical environment. For completeness purposes, we show electron density topology of all conformers in Fig. S4 of the Supporting Information.

So far, we have mainly considered the $n \rightarrow \pi^*$ and $n \rightarrow \sigma^*$ interactions in our discussion. However, as we have pointed out above, these interactions alone cannot explain why the conformer **A1** has a lower energy than ***E1**. In “**Steric effects**,” we discussed the destabilizing contributions to the energy stemming from steric effects.

Fig. 7 Topology of the electron density for the conformers **a A1** and **b *E1**. Medium-sized blue (yellow) spheres depict bond (ring) critical points, and curves composed of small-sized dark blue spheres are bond gradient paths



This analysis included the contribution of all steric effects present in a conformer, i.e., we have subtly suggested that, in the 3NFAC, one cannot identify dominant interactions, but the stabilization is the result of several small different interactions. In this context, QTAIM can shed further light into this.

Ascertain the strength of bonds constitutes an open problem to this day, and there is no unique or straightforward manner to do so. In the present work, we will use the electron density, ρ , evaluated at the bond critical points, hereafter denoted as ρ_{BCP} , an indicator of the bonds' strength. This idea has been applied before for estimating hydrogen bond stabilization energies [27, 28], and here we will conjecture that this relation is also valid for intramolecular interactions.

In “Steric effects,” we discussed how passing from **A1** to ***E1** modifies the portions of the energy that can be associated with steric effects. Here, we will use the electron density, evaluated at the BCPs (associated in turn with standard chemical bonds), in order to qualitatively estimate the changes in the bond strengths of the 3NFAC, and we will suppose that there exists a relation $E_i \propto \rho_{BCP_i}$; here, E_i would be the i th bond stabilization energy. In Fig. S5 of the Supporting Information, we show the difference $\rho_{BCP_i}(\mathbf{A1}) - \rho_{BCP_i}(\mathbf{*E1})$ for all regular bonds of the 3NFAC. We observe that essentially all bonds are affected when passing from **A1** to ***E1**, either increasing or decreasing ρ_{BCP_i} , in such a manner that no general trend can be inferred, i.e., some ρ_{BCP_i} 's increase and some decrease. This is consistent with the discussion presented in “Steric effects,” in the sense that observing a single interaction does not account for the overall stabilization of **A1**. That is, we have to look at the changes suffered by all bonds (even those considered to be far away), interactions, and effects (such as steric or electron delocalization — below).

Ellipticity profiles

Not only every bond and every steric collision are affected when passing from **A1** to ***E1**, but also other more subtle phenomena, such as the electron delocalization and the polar character of some bonds. Again, measuring these effects on a system is an open problem, but we can still extract some useful information using another field derived from the topological properties of the electron density. To this end, in Fig. 8, we show the ellipticity profiles along the bond paths that connect the atoms C2-C11 (Fig. 8a) and C1-C7 (Fig. 8b).

Following closely the results and discussion reported by Cheeseman et al. [29] and Tafipolsky et al. [30], from Fig. 8, we remark the following. The ellipticity profile of the C2-C11 bond shows typical features of a π bond (see Fig. 8a and compare to Fig. 2a of [29]). The maximum of the ellipticity, along the bond path, is close to the critical point (see vertical lines in Fig. 8), which implies that ρ accumulates around the BCP in planes that are perpendicular to the bond path and close to the BCP. Furthermore, since the ellipticity values are, in general, higher in **A1**, we can say that the π character of the of the bond C2-C11 increases, or equivalently that the electron delocalization slightly improves along this bond.

On the other hand, the ellipticity profiles for the bonds C1-C7 of **A1** and ***E1**, respectively, show important differences (see Fig. 8b). The ellipticity profile, for ***E1**, of the bond C1-C7 has roughly the same shape as the bond C2-C11, which implies that the latter bond also has a strong π character. However, the profile, for **A1**, of the bond C1-C7 is less symmetric, and the ellipticity (evaluated at the BCP) is smaller, relative to the conformer ***E1**, which suggests that the bond C1-C7 in **A1** has a weakened π character.

In both **A1** and ***E1**, a local maximum of ε is found close to C7, which indicates that there is a plane around C7 and

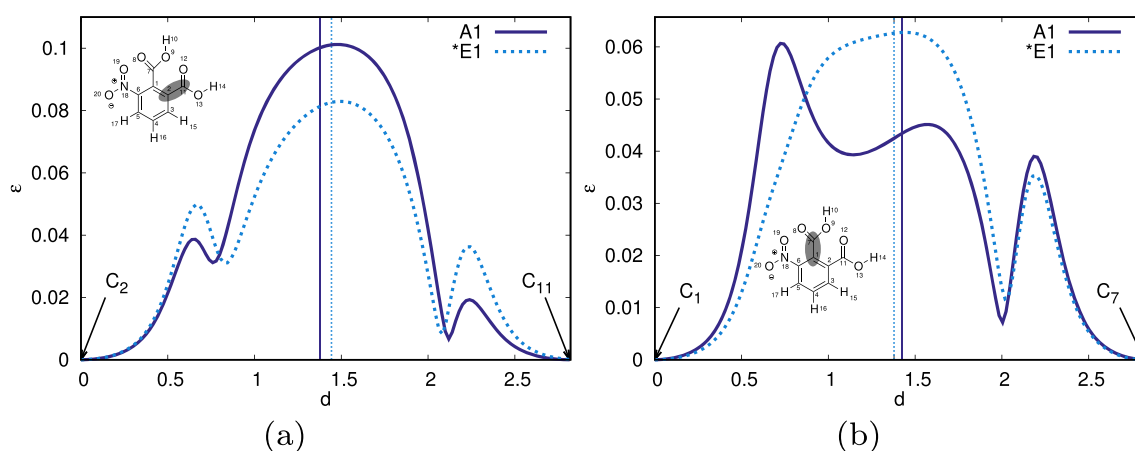


Fig. 8 Ellipticity profiles between **a** C2 and C11 (see shadowed bond of its inset), and **b** C1 and C7 (see shadowed bond of its inset). Solid lines are for the conformer **A1** and dashed lines for ***E1**. Vertical lines indicate the position of the bond critical point along the respective bond gradient path

perpendicular to the bond path; therefore, the π character of the C1-C7 increases nearby the C7 atom. This is consistent with the fact that C7 participates in $n \rightarrow \pi^*$ interactions, i.e., the electron density around C7 increases due to the double $n \rightarrow \pi^*$ interaction.

For complete purposes, we show the ellipticity profile of the bond C6-N18 in Fig. S6 of the Supporting Information. The profiles are quite similar for **A1** and ***E1**, both in shape and height.

Gas vs crystal phases

Quite recently, it has been discussed how much one may extrapolate the observations and results made in gas-phase, as to the $n \rightarrow \pi^*$ interactions, into the designing of molecules in the crystal phase [43]. In this phase, intramolecular interactions may be slightly weakened (relative to the gas phase), in order to allow for both the minimization of intermolecular steric repulsions and the maximization of stabilizing intermolecular interactions, although the total energy of the molecules is almost unaffected. Again, the 3NFAc does not follow exactly the same trend, which is at this point not really surprising because, once more, the crowded electron density around the $-\text{NO}_2$ and both $-\text{COOH}$ groups is tightly coupled, which precludes this molecule to show an intuitive behaviour. For completeness purposes, we performed the NBO, QTAIM, and NCI analyses upon the x-ray structure of the 3NFAc, which we show in Figs. S7 and S8 of the Supplementary Information (computational details for this section are presented in Section 5 of the Supplementary Information).

From Figs. S7 and S8 and Table S1 of the Supplementary Information, we observe that the double $n \rightarrow \pi^*$ interaction is also present in crystal phase, and that the total

energy is barely modified: the difference $E_{\text{Ax}} - E_{\text{A1}} = 1.18 \text{ kcal mol}^{-1}$. (Here, **Ax** is the structure obtained from a partial optimization of the x-ray geometry with $\theta_1 - \theta_5$ frozen, and this does not include ZPE corrections; see Supporting Information for further details.) The latter is consistent with the findings of Breton et al. [43]. However, the $n \rightarrow \pi^*$ interactions are enhanced, as opposed to be weakened: the $E^{(2)}$ of NBO_1 increases by $1.99 \text{ kcal mol}^{-1}$ and the $E^{(2)}$ of NBO_2 increases by $0.89 \text{ kcal mol}^{-1}$, which stems from a greater overlap between the n and π^* orbitals, as adopted in the crystal phase (see and compare Fig. 5a, b and S7 of the Supporting Information). Furthermore, in the crystal configuration, the chemical environment is modified so that the overall intramolecular steric repulsions increase ($S_{\text{Ax}}^{(sx)} - S_{\text{A1}}^{(sx)} = 6.04$). This is not surprising because, in the crystal phase, the 3NFAc's molecules interact through four hydrogen bonds: two $\text{C-H} \cdots \text{O}$ bonds (H17 and $-\text{NO}_2$), and two $\text{O-H} \cdots \text{O}$ bond (H14 and $-\text{COOH}$) [42]. This quadruple intermolecular interaction causes the central $-\text{COOH}$ group to be almost perpendicular to the benenic ring, and the other two groups to be almost co-planar (see Table S1 of the Supplementary information, dihedrals θ_1 , θ_2 and θ_4). This geometric configuration allows the greater overlap of the NBO orbitals, which in turn strengthens the NBO_1 and NBO_2 interactions, and also renders the total steric repulsions to increase, relative to the gas-phase structure **A1**, because the quadruple intermolecular interaction compensates this pair of unstabilizing effects in the crystal phase.

Overall remarks

In addition to the fact that none of the 3NFAc's bonds or interactions determine its structural properties, this molecule constitutes a very interesting case, wherein two

apparently weak non-covalent interactions (each of which of ~ 2.4 kcal mol $^{-1}$) subdue a moderate intramolecular hydrogen bond (of ~ 10 kcal mol $^{-1}$). This outcome is only possible because the intramolecular forces and effects are highly coupled to the dihedral angles ($\theta_1 - \theta_5$) variation. This coupling may be somewhat expected, as the 3NFAc encompasses three highly de-localizable functional groups (namely, one $-\text{NO}_2$ and two $-\text{COOH}$), attached to a benzenic ring, and in consecutive positions. This renders a system with a crowded electron density, which couples the three groups in such a manner that rotating one single dihedral affects not only the immediately surrounding bonds and attractive/repulsive effects, but also modifies the behaviour of farther pieces of the molecule, and even can affect the electron delocalization that involves the benzenic ring. These long-range coupling reflects in a lowest-energy conformer, in which it is preferred the formation of weak $n \rightarrow \pi^*$ interactions over a moderate hydrogen bond, in such a manner that the overall steric repulsion is decreased, at the cost of modifying the electron density of the molecule, and consequently the properties of all individual bonds.

Conclusions

We have presented a theoretical analysis, based on natural bond orbital decomposition, the quantum theory of atoms in molecules, and non-covalent interaction index methodologies, carried out upon all conformers of 3-nitrophthalic acid (3NFAc) that have different total electron energy. The lowest-energy conformer of the 3NFAc is the result of a fragile balance between two intramolecular “weak” interactions of the type $n \rightarrow \pi^*$, the overall steric effects, and the delocalization of the $-\text{NO}_2$ and both $-\text{COOH}$ groups with the benzenic ring. The most salient feature of this molecule is that neither of the previous forces can be considered dominant, in such a manner that two $n \rightarrow \pi^*$ interactions may exist, and be strong enough to overcome the stabilizing effect of an intramolecular hydrogen bond (which is present in more than one of the 3NFAc’s conformers). . . perhaps with a little help from their friends (delocalization and electronic repulsion). The analysis shown here should serve for not to forget that the stability of a molecule is the product of the combined effects of different interactions and forces, and that sometimes, one cannot identify a unique dominant interaction.

Acknowledgements The authors acknowledge Conacyt for LMP’s PhD scholarship (Num. 412202)

Compliance with Ethical Standards

Conflict of interest The authors declare that they have no conflict of interest.


References

- Newberry RW, Raines RT (2017) *Acc Chem Res* 50(8):1838. <https://doi.org/10.1021/acs.accounts.7b00121>. PMID: 28735540
- Singh SK, Das A (2015) *Phys Chem Chem Phys* 17:9596. <https://doi.org/10.1039/C4CP05536E>
- Bürgi HB, Dunitz JD, Shefter E (1974) *Acta Crystallogr B* 30(6):1517. <https://doi.org/10.1107/S0567740874005188>
- Newberry RW, Raines RT (2014) *ACS Chem Biol* 9(4):880. <https://doi.org/10.1021/cb500022u>
- DeRider ML, Wilkens SJ, Waddell MJ, Bretscher LE, Weinhold F, Raines RT, Markley JL (2002) *J Am Chem Soc* 124(11):2497. <https://doi.org/10.1021/ja0166904>. PMID: 11890798
- Bartlett GJ, Choudhary A, Raines RT, Woolfson DN (2010) *Nat Chem Biol* 6:615. <https://doi.org/10.1038/nchembio.406>
- Moraru IT, Petrar PM, Nemeş G (2017) *J Phys Chem A* 121(12):2515. <https://doi.org/10.1021/acs.jpca.7b01208>. PMID: 28282141
- Sandoval-Lira J, Solano-Altamirano J, Cortezano-Arellano O, Cruz-Gregorio S, Meza-León RL, Hernández-Pérez JM, Sartillo-Piscil F (2019) *J Org Chem* 84(4):2126. <https://doi.org/10.1021/acs.joc.8b03116>
- Grabowski S (2006) *Hydrogen bonding - new insights*, 1st edn. Springer, Netherlands. <https://doi.org/10.1007/978-1-4020-4853-1>
- Jeffrey G (1997) *An introduction to hydrogen bonding*. Topics in Physical Chemistry - Oxford University Press. Oxford University Press, Oxford. <https://books.google.com.mx/books?id=ZRAFifo37QsC>
- García-Castro MA, Amador P, Rojas A, Hernández-Pérez JM, Solano-Altamirano J, Flores H, Salas-López K (2018) *J Chem Thermodyn*. <https://doi.org/10.1016/j.jct.2018.07.026>. <http://www.sciencedirect.com/science/article/pii/S0021961418305718>
- Mejía S, Hernández-Pérez JM, Sandoval-Lira J, Sartillo-Piscil F (2017) *Molecules* 22(3). <https://doi.org/10.3390/molecules22030361>. <http://www.mdpi.com/1420-3049/22/3/361>
- Romero-Ibañez J, Cruz-Gregorio S, Sandoval-Lira J, Hernández-Pérez JM, Quintero L, Sartillo-Piscil F (2019) *Angew Chem Int Ed* 58(26):8867. <https://doi.org/10.1002/anie.201903880>. <https://onlinelibrary.wiley.com/doi/abs/10.1002/anie.201903880>
- Newberry RW, Orke SJ, Raines RT (2016) *Org Lett* 18(15):3614. <https://doi.org/10.1021/acs.orglett.6b01655>. PMID: 27409515
- Singh SK, Das A, Breton GW (2016) *J Phys Chem A* 120(31):6258. <https://doi.org/10.1021/acs.jpca.6b03119>
- Choudhary A, Fry CG, Kamer KJ, Raines RT (2013) *Chem Commun* 49:8166. <https://doi.org/10.1039/C3CC44573A>
- Reed AE, Weinstock RB, Weinhold F (1985) *J Chem Phys* 83(2):735. <https://doi.org/10.1063/1.449486>
- Reed AE, Weinhold F (1985) *J Chem Phys* 83(4):1736. <https://doi.org/10.1063/1.449360>
- Foster JP, Weinhold F (1980) *J Am Chem Soc* 102(24):7211. <https://doi.org/10.1021/ja00544a007>
- Bader RFW (1990) *Atoms in molecules: a quantum theory* (International Series of Monographs on Chemistry). Oxford University Press, Oxford
- Johnson ER, Keinan S, Mori-Sánchez P, Contreras-García J, Cohen AJ, Yang W (2010) *J Am Chem Soc* 132(18):6498. <https://doi.org/10.1021/ja100936w>. PMID: 20394428
- Weinhold F (2012) *Discovering chemistry with natural bond orbitals*. Wiley, New York
- Matta CF, Russell JB (2007) *The quantum theory of atoms and molecules. From solid state to DNA and drug design*. Wiley-VCH Verlag GmbH & Co. KGaA, Weinheim
- Contreras-García J, Johnson ER, Keinan S, Chaudret R, Piquemal JP, Beratan DN, Yang W (2011) *J Chem Theory Comput* 7(3):625. <https://doi.org/10.1021/ct100641a>. PMID: 21516178

25. Bader RFW (1991) *Chem Rev* 91(5):893. <https://doi.org/10.1021/cr00005a013>
26. Koch U, Popelier PLA (1995) *J Phys Chem* 99(24):9747. <https://doi.org/10.1021/j100024a016>
27. Parthasarathi R, Subramanian V, Sathyamurthy N (2005) *J Phys Chem A* 109(5):843. <https://doi.org/10.1021/jp046499r>. PMID: 16838955
28. Parthasarathi R, Subramanian V, Sathyamurthy N (2006) *J Phys Chem A* 110(10):3349. <https://doi.org/10.1021/jp060571z>
29. Cheeseman J, Carroll M, Bader R (1988) *Chem Phys Lett* 143(5):450. [https://doi.org/10.1016/0009-2614\(88\)87394-9](https://doi.org/10.1016/0009-2614(88)87394-9). <http://www.sciencedirect.com/science/article/pii/0009261488873949>
30. Tafipolsky M, Scherer W, Öfele K, Artus G, Pedersen B, Herrmann WA, McGrady GS (2002) *J Am Chem Soc* 124(20):5865. <https://doi.org/10.1021/ja011761k>. PMID: 12010062
31. Contreras-García J, Piquemal JP, Miller BJ, Kjaergaard HG (2013) *J Chem Theory Comput* 9(8):3263. <https://doi.org/10.1021/ct400420r>. PMID: 26584086
32. Lane JR, Schröder SD, Saunders GC, Kjaergaard HG (2016) *J Phys Chem A* 120(32):6371. <https://doi.org/10.1021/acs.jpca.6b05898>. PMID: 27447952
33. Johnson ER, Keinan S, Mori-Sánchez P, Contreras-García J, Cohen AJ, Yang W (2010) *J Am Chem Soc* 132(18):6498. <https://doi.org/10.1021/ja100936w>. PMID: 20394428
34. Schmidt MW, Baldrige KK, Boatz JA, Elbert ST, Gordon MS, Jensen JH, Koseki S, Matsunaga N, Nguyen KA, Su S, Windus TL, Dupuis M, Montgomery JA Jr (1993) *J Comb Chem* 14(11):1347. <https://doi.org/10.1002/jcc.540141112>. <https://onlinelibrary.wiley.com/doi/abs/10.1002/jcc.540141112>
35. Glendening ED, Badenhop JK, Reed AE, Carpenter JE, Bohmann JA, Morales CM, Landis CR, Weinhold F (2013) NBO 6.0. Theoretical Chemistry Institute, University of Wisconsin, Madison
36. Zhurko G, Zhurko D (2009) <http://www.chemcraftprog.com>
37. Solano-Altamirano J, Hernández-Pérez JM (2015) *Comput Phys Commun* 196:362. <https://doi.org/10.1016/j.cpc.2015.07.005>. <http://www.sciencedirect.com/science/article/pii/S001046551500274X>
38. Persistence of vision Pty. Ltd., Williamstown, Victoria, Australia. <http://www.povray.org/>
39. Humphrey W, Dalke A, Schulten K (1996) *J Mol Graph* 14:33
40. Tikhonov DS, Sharapa DI, Otyotov AA, Solyankin PM, Rykov AN, Shkurinov AP, Grikina OE, Khaikin LS (2018) *J Phys Chem A* 122(6):1691. <https://doi.org/10.1021/acs.jpca.7b11364>. PMID: 29360361
41. Steiner T (2002) *Angew Chem Int Ed* 41(1):48. [https://doi.org/10.1002/1521-3773\(20020104\)41:1<48::AID-ANIE48>3.0.CO;2-U](https://doi.org/10.1002/1521-3773(20020104)41:1<48::AID-ANIE48>3.0.CO;2-U)
42. Glidewell C, Low JN, Skakle JMS, Wardell JL (2003) *Acta Crystallogr C* 59(3):o144. <https://doi.org/10.1107/S0108270103002555>
43. Breton GW, Davis LO, Martin KL, Chambers TA (2019) *Cryst Growth Des* 19(7):3895. <https://doi.org/10.1021/acs.cgd.9b00322>

Publisher's note Springer Nature remains neutral with regard to jurisdictional claims in published maps and institutional affiliations.

Affiliations

Lorena Monterrosas-Pérez¹ · Jacinto Sandoval-Lira^{2,3} · M. P. Amador-Ramírez¹ · H. Flores-Segura¹ · Julio M. Hernández-Pérez¹ · J. M. Solano-Altamirano¹ 

Lorena Monterrosas-Pérez
lmp3010@gmail.com

Jacinto Sandoval-Lira
jsandovalira@gmail.com

¹ Facultad de Ciencias Químicas, Benemérita Universidad Autónoma de Puebla, 14 Sur y Av. San Claudio, Col. San Manuel, 72520 Puebla, México

² Centro Conjunto de Investigación en Química Sustentable UAEM-UNAM, Carretera Toluca-Atlacomulco Km. 14.5, Unidad San Cayetano, 50200 Toluca de Lerdo, Mexico

³ Instituto de Química, Universidad Nacional Autónoma de México, Circuito Exterior, Ciudad Universitaria, Mexico City, 04510, Mexico